NANO LETTERS

2007
Vol. 7, No. 2
464−469

Block Copolymer Templated Etching on Silicon

Yinghong Qiao, Dong Wang, and Jillian M. Buriak*

Department of Chemistry, University of Alberta and the National Institute for Nanotechnology, National Research Council, Edmonton, AB T6G 2G2, Canada

Received November 28, 2006; Revised Manuscript Received December 20, 2006

ABSTRACT

The use of self-assembled polymer structures to direct the formation of mesoscopic (1–100 nm) features on silicon could provide a fabrication-compatible means to produce nanoscale patterns, supplementing conventional lithographic techniques. Here we demonstrate nanoscale etching of silicon, applying standard aqueous-based fluoride etchants, to produce three-dimensional nanoscale features with controllable shapes, sizes, average spacing, and chemical functionalization. The block copolymers serve to direct the silicon surface chemistry by controlling the spatial location of the reaction as well as concentration of reagents. The interiors of the resulting etched nanoscale features may be selectively functionalized with organic monolayers, metal nanoparticles, and other materials, leading to a range of ordered arrays on silicon.

The fabrication of sub-100 nm features on silicon surfaces is a critical challenge for future technological devices based on silicon-based materials, including hybrid silicon−organic and nanoparticle devices, molecular electronics, micro- and nanofluidics, sensing, photovoltaics, and others.[1,2] The most important representative top-down technique, photolithography, has seen decades of remarkable improvements, leading to the latest 65 nm commercial transistor technologies, with further decreases in size and chip densities still expected.[3] The sheer monetary and energetic costs of manufacturing such devices have reached such an unprecedented magnitude, however, that alternative strategies to produce patterned silicon architectures are under intense investigation in both academia and industry.[3] To be considered commercially viable in the near to mid-term and beyond, new processes should ideally be compatible with existing silicon-based micro- and nanofabrication techniques.

Polymer self-assembly has recently arisen as one possible approach to uniformly pattern large areas of semiconductor interfaces.[4−10] The spontaneous phase separation of block copolymers into nanoscale domains can be harnessed in a cost-effective manner to efficiently and simultaneously produce periodic patterns.[11−16] While certainly not intended to replace photolithography, polymer self-assembly is complementary due in large part to the ubiquity of polymers in IC fabrication processes as photoresists.[4] For instance, IBM announced in 2003 its intention to utilize self-assembled block copolymers that form quasihexagonal close-packed templates for manufacture of floating silicon gates for flash memory. The approach is based upon techniques first described in 1997 in which a block copolymer monolayer serves as a mask for plasma and reactive ion etching.[17]

While the covalent linking of two chemically distinct polymer blocks leads to an amphiphilic molecule, a property critical for the self-assembly process, the dual nature of the polymer can also be used to direct chemical reagents to the surface in a spatially defined manner, as outlined in Figure 1. The chemical specificity of one block over the other toward passage and transport of reagents to the surface results in localized reactivity, directed by the parent block copolymer.[18] The reaction described in this work is based upon the central ingredient in silicon surface processing, the fluoride ion [F^- (aq)], typically derived from either hydrofluoric acid [HF (aq)] or ammonium fluoride [NH_4F (aq)].[19−21] Aqueous fluoride treatment of silicon wafers leads to rapid dissolution of silicon oxide, and depending upon the length of exposure, etching of the silicon lattice and hydride termination.[19,21] Here we demonstrate that self-assembled block copolymer-based quasihexagonal template arrays can direct aqueous fluoride-based etching of silicon surfaces, leading to patterned nanoscale Si−H terminated etch pits on the silicon surface, in minutes, in laboratory ambient. The unetched silicon surface remains terminated by the native oxide, and thus orthogonal chemical functionalization of the etch pits and top silicon interface is possible.

The amphiphilic block copolymer, polystyrene-*block*-poly(4-vinyl pyridine), denoted throughout as PS-*b*-P4VP, was selected as the general polymer for template surface patterning, as illustrated schematically in Figure 1. This block copolymer was chosen because it contains the pyridyl group, a Brönsted base. The sizes of the micellar core (represented in blue) and the corona (represented in red) are easily

* Corresponding author. E-mail: jburiak@ualberta.ca. Telephone: 1-(780)-492-1821. Fax: 1-(780)-492-8231.

10.1021/nl0627801 CCC: $37.00
Published on Web 01/13/2007

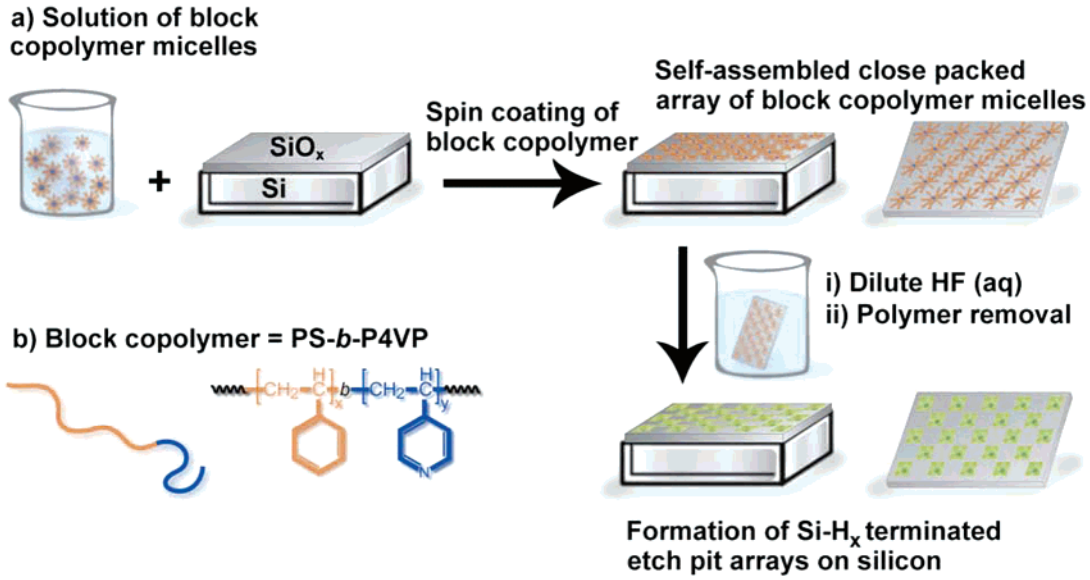

Figure 1. Schematic diagram for the fabrication of the etch pits on a Si(100) surface using PS-*b*-P4VP as the template. (a) The polymer micelles solution formed in toluene were spin-coated onto a native oxide-coated silicon surface, and the micelles spontaneously self-assembled into a quasihexagonal close-packed monolayer array on the surface. Next, the polymer thin film coated silicon shard was dipped into an HF (aq) solution for the designated time. The etch pit array (squares shown here) was obtained after removal of the polymer. (b) Chemical structure of the PS-*b*-P4VP block copolymer.

controlled through variation of the molecular weight of two blocks.[22] The micelles are transferred from solution onto the Si surface by spin-coating or dip-coating, upon which they spontaneously self-assemble into monolayers of quasihexagonal arrays, thus resulting in formation of the template for the subsequent etching process. Through immersion of native oxide-capped Si wafers of different orientations, coated with a monolayer of the self-assembled PS-*b*-P4VP block copolymer [PS-*b*-P4VP, (M_n = 128 400-*b*-33 500 g/mol)] in a dilute HF (aq) solution for less than 1 h, etching of the silicon surface takes place selectively in a manner that reflects the spacing of the parent template. As shown in the plane and sectional view scanning electron microscopy (SEM) images of polymer-coated Si wafer shard dipped in 0.01% HF (aq) for 40 min (Figure 2), the etch pits develop underneath the P4VP cores of the block copolymer film. After removing polymer film by 5 min ultrasonication of the wafer shard in neat toluene, the well-defined etch pit array is revealed. Plan view SEM images (Figure 3a−d) of Si(100), Si(111), and Si(110) show the formation of truncated square and pseudohexagonal-shaped etch pits with center-to-center spacings of ∼125 nm, identical to that of the parent block copolymer monolayer. The cross-sectional images in Figure 3e−h reveal the three-dimensional nature of the etch pits, each defined by apparently flat walls that can be assigned to Si(111), Si(100), and possibly transitional Si-(311) faces (Figure 3i−l, vide infra).[23,24] Some degree of corner rounding is apparent, as is common in the absence of a clearly defined top surface mask.[23] Oxygen appears to play a minor role, as shown by the subtle difference in etch pit shapes on Si(100) in the presence and absence of oxygen (Figures 3a−b). Oxygen is an anisotropic oxidant of Si-(111)−H surfaces, and thus its occurrence appears to have a minor role in etch pit morphology.[25]

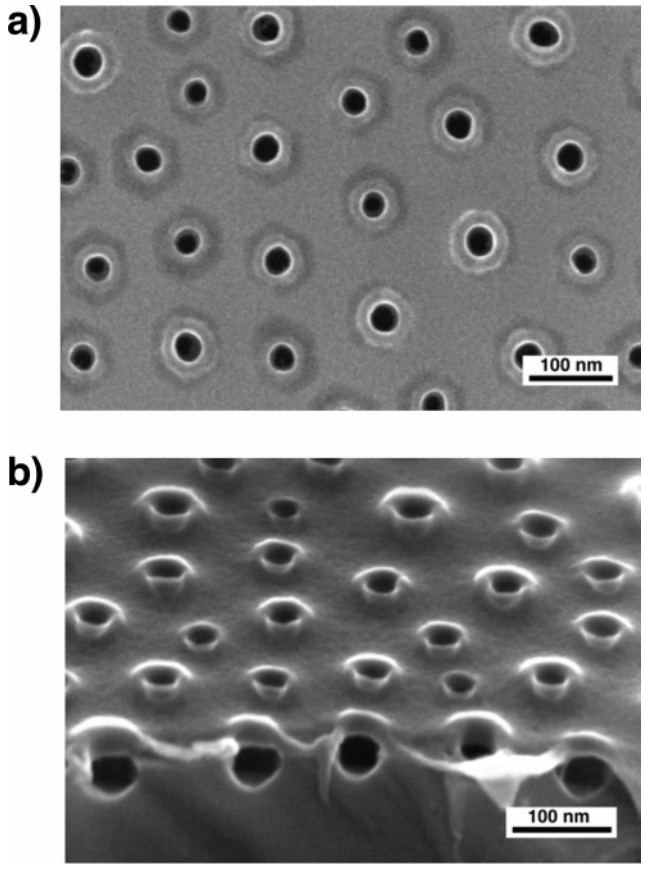

Figure 2. Morphology of the copolymer template coated surface after immersion into HF (aq) solution. Top (a) and side (b) view SEM images of a PS-*b*-P4VP(128 400-*b*-33 500) coated Si(111) surface etched in 0.01% HF (aq) for 40 min, with the polymer left intact; the polymer removal step was omitted.

Etching takes place exclusively beneath the micellar cores, in close proximity to the P4VP cores due to protonation of

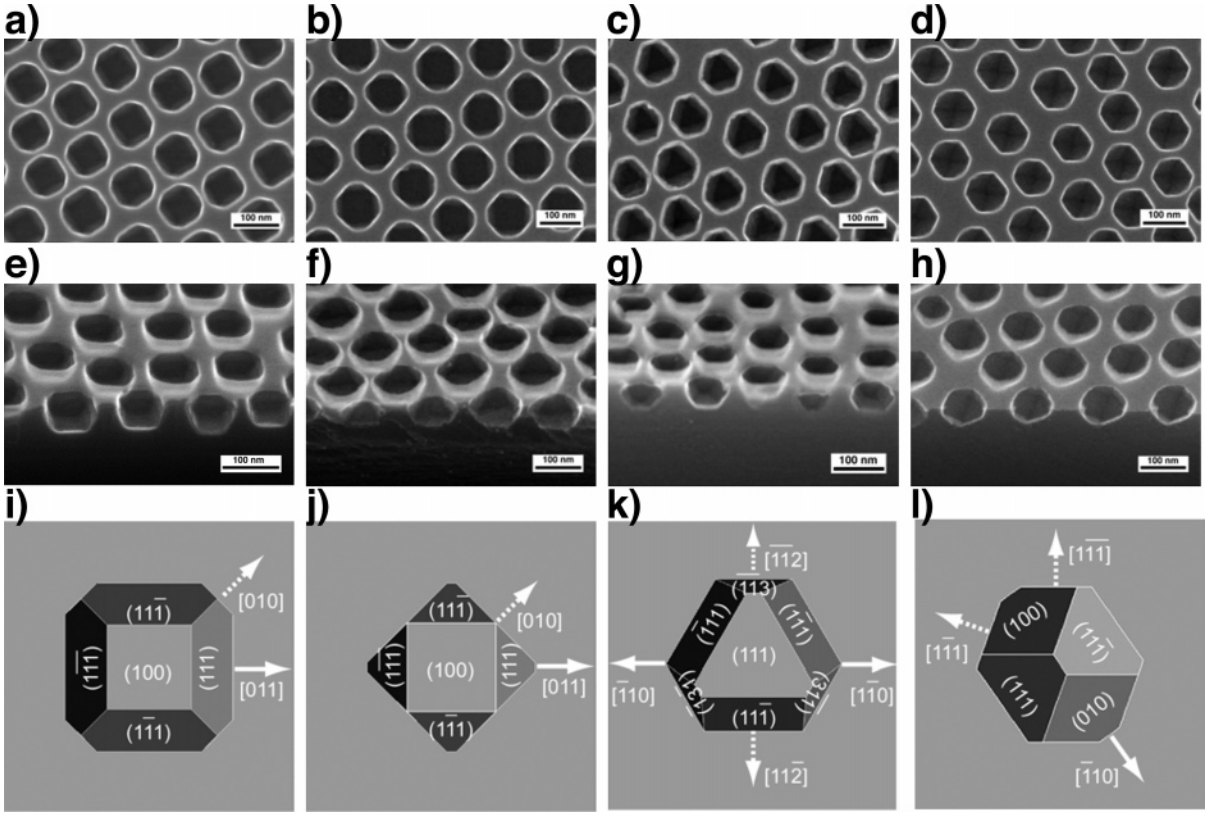

Figure 3. Geometric shape evolution of the patterned etch pits on different orientations of single crystalline silicon. Top (a−d) and side (e−h) view SEM images showing the etch pit arrays on silicon. (a and e) Etching of Si(100), in 0.01% HF (aq) for 50 min, in air. (b and f) Si(100) etched in Ar sparged 0.01% HF (aq) for 50 min. (c and g) Si(111) etched in Ar sparged 0.01% HF (aq) for 40 min. (d and h) Si(110) etched in Ar sparged 0.01% HF (aq) for 40 min. (i−l) Top view models showing the proposed assignments of the exposed planes of the etch pits.

the pyridyl groups of the poly(4-vinylpyridine) block by HF ($pK_a = 3.17$) that results in selective localization of fluoride ion within the P4VP core. The resulting high local concentration of (poly)pyridinium fluoride at the silicon surface is reminiscent of the well-studied ammonium fluoride (aq) etchant, typically used at high concentrations (~40% w/w in water). Ammonium fluoride (aq) is an anisotropic etchant that etches much more slowly along the ⟨111⟩ direction than along the ⟨100⟩ direction.[26,27] On Si(111) surfaces, anisotropic etching with NH_4F (aq) leads to atomically flat, monohydride-terminated Si(111) interfaces, while it has been reported that on Si(100), a rougher interface made up of Si(111)−H microfacets and Si(100)−H_2 planes is produced.[28,29] To demonstrate that the poly(pyridinium) fluoride block could be the etchant, a 56% w/w pyridinium fluoride (aq) solution was studied for the etching of the Si(100), Si(111), and Si(110) wafers (SEM images in Supporting Information). Similar square and elongated pseudohexagonal pit shapes and morphologies are observed on Si(100) and Si(110) surfaces, respectively, although their sizes and locations are diverse and heterogeneous due to the obvious lack of spatial control. On the other hand, triangular etch pits form on Si(111) with the 56% pyridinum fluoride (aq) solution; triangular and pseudohexagonal etch pits are simply variations on the same theme and are closely related as the two morphologies differ only in the rate of etching of the Si(11$\bar{2}$) and Si($\bar{1}\bar{1}$2) planes.[30,31] The three broad internal walls of the pseudohexagonal etch pit structures can be assigned as Si(111) faces (Figure 3k), identical to the three walls of the triangular etch pits.[32] The three smaller walls, on the other hand, are more difficult to assign because formation of the stable Si(111) face would result in undercutting, as has been observed in other basic etches.[33] A provisional assignment of an intermediary Si(311) surface would yield an almost vertical wall [~80° from surface Si(111) plane], similar to those observed here by SEM (Figure 3g); the Si(311) face should be considered to be composed of stairlike ledges of Si(100) and Si(111) planes.[23] The morphological shapes of the etch pits are transitional, and thus a particular form observed at any given time represents the arrested development of the anisotropic etching reaction; the shapes may not correspond to the most stable final product of the etching solution [hence the appearance of atypical surfaces such as the proposed Si(311) faces, for instance].

Evolution of the morphology of etch pits through simple modulation of immersion time and HF concentration allows access to a range of shapes and sizes. Preliminary screening revealed the importance of HF concentration with respect to both the size and shape of the etch pits as well as etching rates because both are affected dramatically over the range from 10% to 0.01% HF (aq) (Supporting Information); little etching and etch pit formation was observed below 0.01% HF (aq) concentration. Parts a−d and e−h of Figure 4 show the SEM images of etch pits on Si(100) and Si(111),

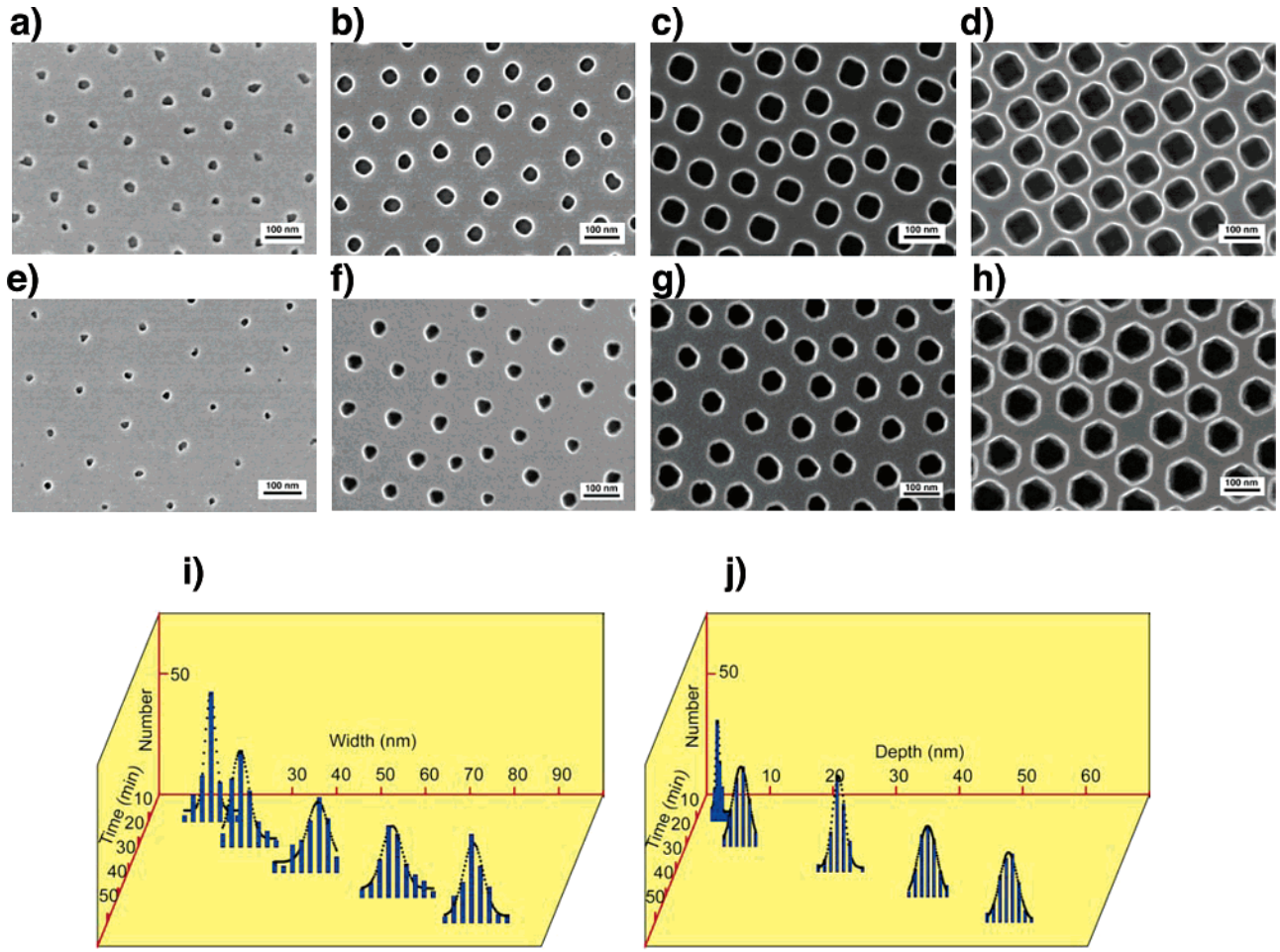

Figure 4. Shape evolution of etch pits with increasing etching time. SEM images of the etch pits on Si(100) (a−d) and Si(111) (e−h) obtained at different etching time using PS-*b*-P4VP (M_n = 128 400-*b*-33 500 g/mol) as templates. The etching time from (a−d) is 20, 30, 40, and 50 min, respectively. The etching time from (e−h) is 10, 20, 30, and 40 min, respectively. HF (aq) solution (0.01%) was used as etchant in all cases. (i and j) Histogram representation of the width and depth distribution of the etch pits obtained with different etching times on Si(100).

respectively, obtained at increasing etching times using PS-*b*-P4VP (M_n = 128 400-*b*-33 500 g/mol) as a template in 0.01% HF (aq). The SEM images and the histograms in Figure 4i−j for Si(100) show that the etch pit diameter varied from ∼14 to ∼83 nm with increasing time; the depth of the etch pits also simultaneously increased from <5 to ∼55 nm. In addition to the increase in depth and width, the morphology of etch pits also evolved, starting with irregularly shaped pits at short etching times, and gradually developing into well-defined geometric shapes after 30−40 min. The kinetics of etching in this system are influenced not only by silicon etching parameters but also by inversion of the PS-*b*-P4VP block copolymer in acid. As has been previously reported, immersion of a monolayer of PS-*b*-P4VP in methanol or ethanol results in inversion of the structure,[34,35] and AFM images taken after exposure to HF (aq) also show a similar inversion phenomenon (Supporting Information). The morphological shift of the PS-*b*-P4VP block copolymer would be expected to affect local concentrations of fluoride ion; the influence of polymer inversion on silicon etching kinetics is clearly complex and will be the subject of further study.

In addition to shape, diameter, and depth, periodicity can be controlled through utilization of block copolymers of different molecular weights. Parts a−c of Figure 5 show atomic force microscopy (AFM) images of PS-*b*-P4VP with molecular weights of PS-*b*-P4VP (M_n = 20 000-*b*-19 000 g/mol), PS-*b*-P4VP (M_n = 57 300-*b*-24 700 g/mol), and PS-*b*-P4VP (M_n = 128 400-*b*-33 500 g/mol); the center-to-center spacings of the P4VP cores, the bright spots in the AFM images, vary from 50 to 65 to 125 nm, respectively. The corresponding film thickness of each block copolymer film for each of the three molecular weights was 23 ± 1, 30 ± 1, and 23 ± 1 nm, respectively, as measured by ellipsometry (Supporting Information). Brief immersion the PS-*b*-P4VP monolayer-capped silicon wafer in 1% HF (aq) for 3 min, followed by polymer removal through 5 min of ultrasonication in toluene, results in etch pits on the surface with identical periodicity to that of the parent polymer template (Figure 5d−f).

Precise control over the chemistry of the internal environment of the etch pits would enable, for instance, selective functionalization, growth, and isolation of nanoscale materials and immobilization of individual biomolecules. Because fluoride-based etching of Si(s) yields surface-bound Si−H_x groups, the walls of the etch pits would be expected to be hydride-terminated. The PS layer prevents contact of the HF

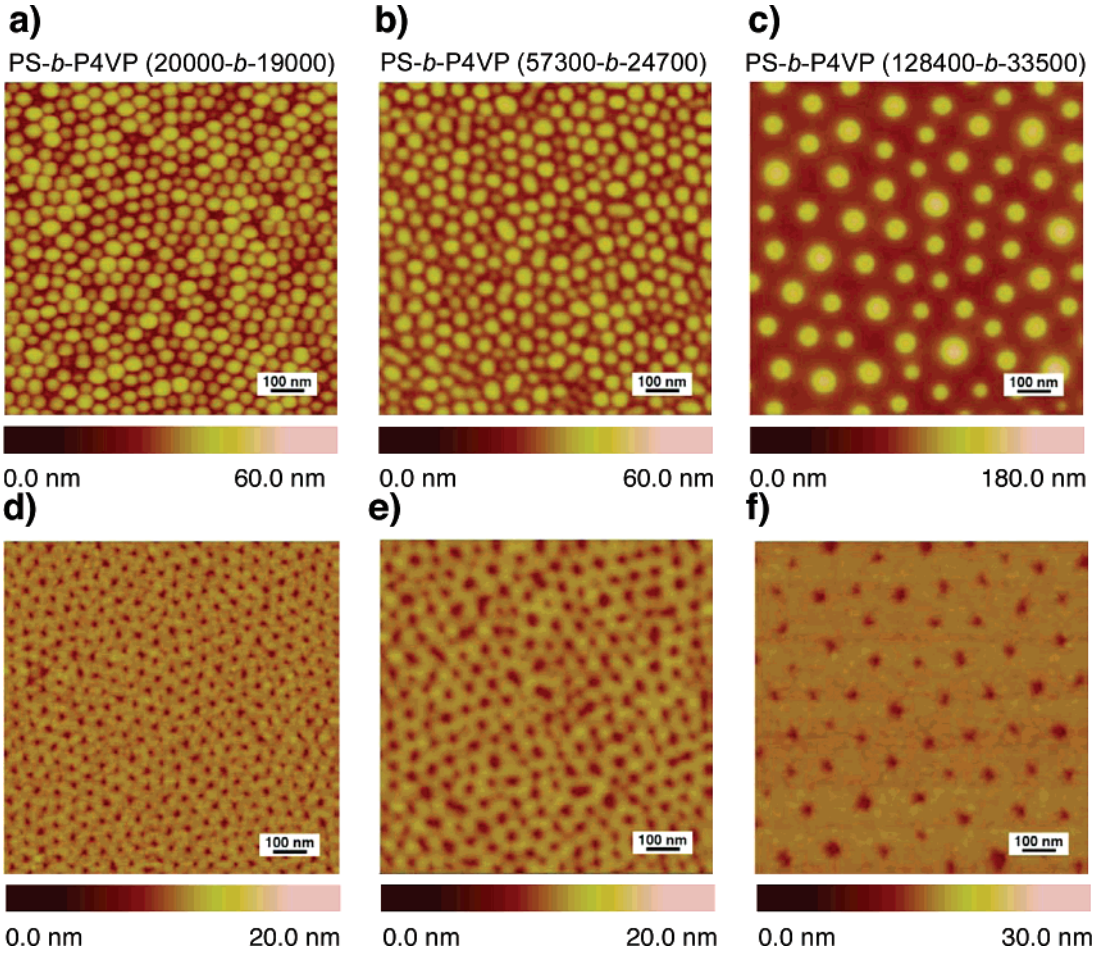

Figure 5. Modulation of etch pit periodicity by using block copolymers of different molecular weights. (a−c) AFM height images of PS-*b*-P4VP (*x*-*b*-*y*) thin films on a silicon (100) surface, where *x* and *y* designate the molecular weights of the PS and P4VP blocks, respectively. (d−f) AFM height images of the corresponding patterned etch pits obtained by etching with 1% HF (aq) for 3 min. Scan areas are 1 μm × 1 μm in all cases.

etching solution with the native oxide on the silicon surfaces, leading to exclusive etch pit formation under the P4VP cores; the top unetched silicon surface should therefore remain oxide terminated. As a result, selective functionalization either inside the etch pits or on the top oxide surface should be achievable, assuming that the etching process is indeed as selective as postulated. Germanium attenuated total reflection IR (GATR) of a Si(100) surface etched with 1% HF (aq) through a PS-*b*-P4VP monolayer has both nonoxidized and oxygen back-bonded ν(Si−H_x) modes centered around 2100−2200 cm^{-1} (Supporting Information). The two modes would be expected, as there are at least two populations of Si−H_x groups, one near the oxide interface and the other on the nonoxidized Si−H_x terminated etch pit interior. Si−H_x termination of the pore interiors can be demonstrated via galvanic reduction of $HAuCl_4$ to Au(0) nanoparticles (Supporting Information). Galvanic displacement reactions, widely studied as a means to deposit metals on semiconductor surfaces, will occur spontaneously on H-terminated Si surfaces and not on the insulating oxide interface.[36−38] A freshly patterned Si(100) wafer, following removal of the block copolymer, was immersed in a $HAuCl_4$ (10^{-4} M) ethanolic solution (H_2O/ethanol = 1:1, v/v) for 5 min.[36] Strongly adhering gold nanoparticles grew selectively inside the etch pits with no metal observed on the oxide interface, demonstrating the obvious difference in chemical reactivity between the etch pit interior and the flat top surface due to the distinct functionalities, oxide versus hydride. The Si−H_x terminated etch pit interiors may also be functionalized via hydrosilylation of a long chain alkyne, producing Si−alkenyl groups,[39,40] as confirmed by the production of ν(C−H_x) modes (Supporting Information). Because the chemistry of silicon surfaces is now so diverse,[41,42] the possibilities to interface a wide variety of functional molecules and structures, both within the etch pit and on the top face, are endless.

In conclusion, block copolymer-directed silicon surface etching is demonstrated, using an only aqueous fluoride-based chemical etchants. Through modulation of the etching conditions (time, fluoride concentration, silicon wafer orientation, etc.), shape, size, and morphology of the resulting etch pits can be controlled. Because fluoride etching of silicon results in hydride termination, the etch pit interiors are chemically distinct from the top face of the silicon wafer, rendering it possible to construct functionalized three-dimensional etched nanostructures on the wafer. Fluoride-based etching, mediated by a variety of self-assembled block copolymer structures, is presently underway.

Acknowledgment. This work was supported by the National Research Council (NRC) of Canada, the University of Alberta, NSERC, and the Canadian Foundation for Innovation. We are thankful for the technical support provided at the National Institute for Nanotechnology (NINT) and the Alberta Centre for Surface Engineering and Science (ACSES) at the University of Alberta.

Supporting Information Available: Detailed experimental procedures, additional SEM images of the etched surfaces, AFM images of the block copolymer upon treatment with HF (aq), IR spectra of the hydride- and alkenyl-terminated surfaces, and side-view of the etch pit models. This material is available free of charge via the Internet at http://pubs.acs.org.

References

(1) Xia, Y.; Rogers, J. A.; Paul, K. E.; Whitesides, G. M. *Chem. Rev.* **1999**, *99*, 1823−1848.
(2) Barth, J. V.; Costantini, G.; Kern, K. *Nature* **2005**, *437*, 671−679.
(3) The ITRS Roadmap, found at http://www.itrs.net under "reports".
(4) Guarini, K. W.; Black, C. T.; Zhang, Y.; Kim, H.; Sikorski, E. M.; Babich. I. V. *J. Vac. Sci. Technol., B: Microelectron. Nanometer Struct.—Process., Meas., Phenom.* **2002**, *20*, 2788−2792.
(5) Black, C. T. *Appl. Phys. Lett.* **2005**, *87*, 163116.
(6) Hawker, C. J.; Russell, T. P. *MRS Bull.* **2005**, *30*, 952−966.
(7) (a) Glass, R.; Möller, M.; Spatz, J. P. *Nanotechnology* **2003**, *14*, 1153−1160. (b) Kästle, G.; Boyen, H. G.; Weigl, F.; Lengl, G.; Herzog, T.; Ziemann, P.; Riethmüller, S.; Mayer, O.; Hartmann, C.; Spatz, J. P.; Möller, M.; Ozawa, M.; Banhart, F.; Garnier, M. G.; Oelhafen, P. *Adv. Funct. Mater.* **2003**, *13*, 853−861. (c) Spatz, J. P.; Mössmer, S.; Hartmann, C.; Möller, M.; Herzog, T.; Krieger, M.; Boyen, H. G.; Ziemann, P.; Kabius, B. *Langmuir* **2000**, *16*, 407−415. (d) Spatz, J. P.; Herzog, T.; Mössmer, S.; Ziemann, P.; Möller, M. *Adv. Mater.* **1999**, *11*, 149−153. (e) Spatz, J. P.; Sheiko, S.; Möller, M. *Adv. Mater.* **1996**, *8*, 513−517.
(8) La, Y. H.; Edwards, E. W.; Park, S. M.; Nealey, P. F. *Nano Lett.* **2005**, *5*, 1379−1384.
(9) (a) Mansky, P.; Chaikin, P.; Thomas, E. L. *J. Mater. Sci.* **1995**, *30*, 1987−1992. (b) Cheng, J. Y.; Ross, C. A.; Chan, V. Z.-H.; Thomas, E. L.; Lammertink, R. G. H.; Vancso, G. J. *Adv. Mater.* **2001**, *13*, 1174−1178. (c) Cheng, J. Y.; Ross, C. A.; Thomas, E. L.; Smith, H. I.; Vancso, G. J. *Appl. Phys. Lett.* **2002**, *81*, 3657−3659.
(10) Park, M.; Harrison, C.; Chaikin, P. M.; Register, R. A.; Adamson, D. H. *Science*, **1997**, *276*, 1401−1404.
(11) Antonietti, M.; Göltner. C. *Angew. Chem., Int. Ed.* **1997**, *36*, 910−928.
(12) Hamley, I. W. *Angew. Chem., Int. Ed.* **2003**, *42*, 1692−1712.
(13) Aizawa, M.; Buriak, J. M. *J. Am. Chem. Soc.* **2005**, *127*, 8932−8933.
(14) Lin, Z. Q.; Kim, D. H.; Wu, X. D.; Boosahda, L.; Stone, D.; LaRose, L.; Russell, T. P. *Adv. Mater.* **2002**, *14*, 1373−1376.
(15) Yang, X. M.; Xiao, S. G.; Liu, C.; Pelhos, K.; Minor, K. *J. Vac. Sci. Technol., B: Microelectron. Nanometer Struct.—Process., Meas., Phenom.* **2004**, *22*, 3331−3334.
(16) Stoykovich, M. P.; Müller, M.; Kim, S. O.; Solak, H. H.; Edwards, E. W.; de Pablo, J. J.; Nealey, P. F. *Science* **2005**, *308*, 1442−1446.
(17) Mansky, P.; Liu, Y.; Huang, E.; Russell, T. P.; Hawker, C. *Science* **1997**, *275*, 1458−1460.
(18) Aizawa, M.; Buriak, J. M. *J. Am. Chem. Soc.* **2006**, *128*, 5877−5886.
(19) Monk, D. J.; Soane, D. S.; Howe, R. T. *Thin Solid Films* **1993**, *232*, 1−12.
(20) Lehmann, V. *Electrochemistry of Silicon: Instrumentation, Science, Materials and Applications*; Wiley-VCH: New York, 2002.
(21) Higashi, G. S.; Chabal, Y. J.; Trucks, G. W.; Raghavachari, K. *Appl. Phys. Lett.* **1990**, *56*, 656−658.
(22) Förster, S.; Zisenis, M.; Wenz, E.; Antonietti, M. *J. Chem. Phys.* **1996**, *104*, 9956−9970.
(23) Resnik, D.; Vrtacnik, D.; Amon, S. *J. Micromech. Microeng.* **2000**, *10*, 430−439.
(24) Resnik, D.; Vrtacnik, D.; Aljancic, U.; Amon, S. *J. Micromech. Microeng.* **2003**, *13*, 26−34.
(25) Garcia, S. P.; Bao, H.; Manimaran, M.; Hines, M. A. *J. Phys. Chem. B* **2002**, *106*, 8258−8264.
(26) Hines, M. A. *Annu. Rev. Phys. Chem.* **2003**, *54*, 29−56.
(27) Faggin, M. F.; Green, S. K.; Clark, I. T.; Queeney, K. T.; Hines, M. A. *J. Am. Chem. Soc.* **2006**, *128*, 11455−11462.
(28) Neuwald, U.; Hessel, H. E.; Feltz, A.; Memmert, U.; Behm, R. J. *Surf. Sci.* **1993**, *296*, L8−L14.
(29) Thanh, V. L.; Bouchier, D.; Débarre, D. *Phys. Rev. B* **1997**, *56*, 10505−10509.
(30) Flidr, J.; Huang, Y.-C.; Newton, T. A.; Hines, M. A. *J. Chem. Phys.* **1998**, *108*, 5542−5553.
(31) Gosálvez, M. A.; Nieminen, R. M. *New J. Phys.* **2003**, *5*, 100.1−100.28.
(32) Oosterbroek, R. E.; Berenschot, J. W.; Jansen, H. V.; Nijdam, A. J.; Pandraud, G.; van den Berg, A.; Elwenspoek, M. C. *J. Microelectromech. Syst.* **2000**, *9*, 390−398.
(33) Famini, S.; Esfandyarpour, B.; Mohajerzadeh, S. *J. Electrochem. Soc.* **2006**, *153*, G721−G725.
(34) Sohn, B.-H.; Yoo, S.-I.; Seo, B.-W.; Yun, S.-H.; Park, S.-M. *J. Am. Chem. Soc.* **2001**, *123*, 12734−12735.
(35) Krishnamoorthy, S.; Pugin, R.; Brugger, J.; Heinzelmann, H.; Hoogerwerf, A. C.; Hinderling, C. *Langmuir* **2006**, *22*, 3450−3452.
(36) Magagnin, L.; Maboudian, R.; Carraro, C. *J. Phys. Chem. B* **2002**, *106*, 401−407.
(37) Niwa, D.; Homma, T.; Osaka, T. *J. Phys. Chem. B* **2004**, *108*, 9900−9904.
(38) Lin, H. H.; Mock, J.; Smith, D.; Gao, T.; Sailor, M. J. *J. Phys. Chem. B* **2004**, *108*, 11654−11659.
(39) Sieval, A. B.; Vleeming, V.; Zuilhof, H.; Sudhölter, E. J. R. *Langmuir* **1999**, *15*, 8288−8291.
(40) Linford, M. R.; Fenter, P.; Eisenberger, P. M.; Chidsey, C. E. D. *J. Am. Chem. Soc.* **1995**, *117*, 3145−3155.
(41) Buriak, J. M. *Chem. Rev.* **2002**, *102*, 1271−1308.
(42) Onclin, S.; Ravoo, B. J.; Reinhoudt, D. N. *Angew. Chem., Int. Ed.* **2005**, *44*, 6282−6304.

NL0627801